



OPEN

Genome-wide transcriptome analysis of the orphan crop tef (*Eragrostis tef* (Zucc.) Trotter) under long-term low calcium stress

Ayalew Ligaba-Osena^{1,7}✉, Mohammad Salehin^{1,7}, Muhammad Numan¹, Xuegeng Wang^{2,3}, Sang-Chul Choi¹, Dereje Jima⁴, Louis-Marie Bobay⁵ & Wanli Guo^{1,6}

Calcium (Ca²⁺) is one of the essential mineral nutrients for plant growth and development. However, the effects of long-term Ca²⁺ deficiency in orphan crops such as Tef [*Eragrostis tef* (Zucc.) Trotter], which accumulate high levels of Ca in the grains, remained unknown. Tef is a staple crop for nearly 70 million people in East Africa, particularly in Ethiopia and Eritrea. It is one of the most nutrient-dense grains, and is also more resistant to marginal soils and climatic conditions than main cereals like corn, wheat, and rice. In this study, tef plants were grown in a hydroponic solution containing optimum (1 mM) or low (0.01 mM) Ca²⁺, and plant growth parameters and whole-genome transcriptome were analyzed. Ca²⁺-deficient plants exhibited leaf necrosis, leaf curling, and growth stunting symptoms. Ca²⁺ deficiency significantly decreased root and shoot Ca, potassium (K), and copper content in both root and shoots. At the same time, it greatly increased root iron (Fe) content, suggesting the role of Ca²⁺ in the uptake and/or translocation of these minerals. Transcriptomic analysis using RNA-seq revealed that members of Ca²⁺ channels, including the cyclic nucleotide-gated channels and glutamate receptor-like channels, Ca²⁺-transporters, Ca²⁺-binding proteins and Ca²⁺-dependent protein kinases were differentially regulated by Ca²⁺ treatment. Moreover, several Fe/metal transporters, including members of vacuolar Fe transporters, yellow stripe-like, natural resistance-associated macrophage protein, and oligo-peptide transporters, were differentially regulated between shoot and root in response to Ca²⁺ treatment. Taken together, our findings suggest that Ca²⁺ deficiency affects plant growth and mineral accumulation by regulating the transcriptomes of several transporters and signaling genes.

Calcium (Ca²⁺) is an essential plant nutrient with two crucial roles. It is a structural component of the cell wall and membranes¹ where it binds to an acidic group of the membrane lipids and crosslinks pectin². Ca²⁺ also acts as a ubiquitous second messenger in environmental stress signaling^{1,3}. Several environmental stimuli lead to the release of stored Ca²⁺, which binds to calmodulin. The Ca²⁺-calmodulin complex recruits several kinases and phosphatases that regulate transcription-dependent cellular processes⁴. Plant cells also possess other Ca²⁺-regulated proteins, including Ca²⁺ dependent protein kinase (CDPKs), calcineurin B-like (CBL) proteins, CBL interacting protein kinases (CIPKs), CDPK-related kinases (CRKs), etc., which have been well characterized^{5,6}.

In plants, Ca²⁺ is taken up from the soil solution by roots and translocated to the shoot via the xylem⁴. Ca²⁺ enters plant cells through Ca²⁺ channels⁴. Plant glutamate receptor-like (GLR) channels, which are analogs to the mammalian ionotropic glutamate receptors (iGluRs), are implicated in Ca²⁺ sensing, signaling, and

¹Laboratory of Plant Molecular Biology and Biotechnology, Department of Biology, University of North Carolina Greensboro, Greensboro, NC, USA. ²Laboratory of Environmental Epigenetics, Department of Biology, University of North Carolina Greensboro, Greensboro, NC, USA. ³Institute of Modern Aquaculture Science and Engineering, College of Life Sciences, South China Normal University, Guangzhou 510631, People's Republic of China. ⁴Center of Human Health and the Environment (CHHE) and Bioinformatics Research Center (BRC), North Carolina State University, Raleigh, NC 27606, USA. ⁵Laboratory of Microbial Genomics and Evolution, Department of Biology, University of North Carolina Greensboro, Greensboro, NC, USA. ⁶Department of Biotechnology, College of Life Sciences and Medicine, Zhejiang Sci-Tech University, Hangzhou, People's Republic of China. ⁷These authors contributed equally: Ayalew Ligaba-Osena and Mohammad Salehin. ✉email: alosena@uncg.edu

long-distance root to shoot Ca^{2+} wave propagation during wounding^{7,8}. Several members of the AtGLRs have been characterized^{9,10}. The role of AtGLR3.1 in Ca^{2+} sensing in Arabidopsis shoot has been reported¹¹. Another class of Ca^{2+} channels known as cyclic nucleotide-gated channels (CNGCs) has also been implicated in Ca^{2+} transport^{12,13}. Cellular Ca^{2+} concentration is tightly regulated to allow signaling role, control Ca^{2+} translocation to the shoot and prevent cation toxicity⁴. Antiporters, uniporters and Ca^{2+} -ATPases localized in all major plant cellular membranes and rapidly expel Ca^{2+} from the cytosol. The Arabidopsis genome encodes five different Ca^{2+} efflux systems, called autoinhibited Ca^{2+} -ATPases (ACAs), ER-type Ca^{2+} ATPases (ECAs), and P1-ATPases (HMA1), the mitochondrial calcium uniporter complex (MCUC) and Ca^{2+} exchangers (CAX)^{14,15}. Similarly, Ca^{2+} /Cation-exchangers have also been reported to play a role in cation homeostasis in plants^{16,17}.

Ca^{2+} deficiency is not commonly observed in most soils due to its relative abundance and regular liming practice^{1,18}. However, developing tissues may experience Ca^{2+} deficiency due to lack of Ca^{2+} remobilization from older tissues, under conditions of low transpiration, in sandy soils untreated with lime (CaCO_3 or $\text{Ca}(\text{OH})_2$), and inhibition of Ca^{2+} uptake due to competition from other cations^{1,18}. Plants exposed to Ca^{2+} deficiency may experience necrosis of the meristems, shoot and root growth stunting⁴ and leaf curling. Ca^{2+} -deficiency increases the level of reactive oxygen species, causing oxidative stress in high Ca-demanding plant species such as cabbage^{19,20} and broccoli²¹. Ca^{2+} treatment has been shown to enhance the antioxidant system and decrease oxidative stress in plants grown under high temperature²², drought²³, salinity²⁴ and heavy metals²⁵.

Calcium-sensing networks, including the calcineurin B-like proteins (CBL)-CBL-interacting protein kinase (CIPK), has been implicated in plant abiotic stresses, including K^+ -deficiency²⁶. The CBL1/9—CIPK23 has been implicated in the regulation of K^+ ²⁷ and Fe homeostasis (41). Similarly, CBL1/CBL9-CIPK11 interaction has been involved in regulating the bHLH transcription factor FIT, a crucial regulator of Arabidopsis Fe acquisition²⁸. Fe deprivation has been linked to alteration of Ca^{2+} signatures evoked by exogenous ATP²⁹, suggesting crosstalk between Ca^{2+} and Fe homeostasis. However, detailed studies on the interconnection between Ca^{2+} and Fe nutrition are missing. Recently, studies of factors modulating Ca^{2+} -iron homeostasis are emerging^{29,30}.

Tef is an important orphan crop in the Horn of Africa^{31,32} and some other countries including the United States where it is grown primarily for animal feed³³. Recently, tef has been getting increased attention in many laboratories due to its health benefits and potential roles in sustainable agriculture^{32,34}. Its mineral nutrient composition has been studied³⁵. Tef is one of the orphan crops reported to have higher mineral contents; mainly, the Ca^{2+} content of tef is higher than other crops such as sorghum, barley, wheat, and rice³⁶. The Ca^{2+} content in the plant varies from 0.1 to 5% of the shoot dry weight⁴ and the average seed Ca^{2+} content may vary between 981 and 1811 mg/Kg in tef as compared to 33 mg/Kg in maize, 153 mg/Kg in rice and 533 mg/Kg in wheat³⁵.

Similarly, in millets such as finger millet, the Ca^{2+} contents were higher than in other major crops such as wheat, rice, and maize³⁷. Low Ca^{2+} consumption in the diet has been related to several disorders in humans, many of which can have significant health repercussions over time. Because most staple food grains are low in Ca^{2+} , tef, which is an orphan crop with high Ca^{2+} content, has enormous promise as a nutritional security crop. However, orphan crops' physiological and transcriptomic response to Ca^{2+} nutrition has not been studied before.

This study exposed tef plants to long-term Ca^{2+} deficiency and analyzed the physiological and transcriptomic responses. Our findings revealed that prolonged low Ca^{2+} treatment decreased shoot and root biomass, Ca, K, and copper (Cu) content while significantly suppressing Fe translocation from the roots to the shoot. Transcriptomic analysis using RNA-seq revealed that some members of Ca^{2+} transporters, including CNGC, GLR and CaUP, signaling genes such as CBP and CDPK and genes implicated in Fe homeostasis such as YSL, OPT, VIT and NRAMP are differentially regulated by Ca^{2+} treatment or between roots and shoots.

Results

Low Ca^{2+} treatment inhibits plants growth. To understand the effect of long-term Ca^{2+} deficiency in tef, plants were grown in a modified Hoagland's hydroponic solution supplemented with predetermined low (0.01 mM) or optimum (1 mM) Ca^{2+} for one month, and the plants were analyzed. As shown in Fig. 1, plants grown in low Ca^{2+} exhibited typical Ca^{2+} deficiency symptoms, including leaf tip necrosis and growth stunting, compared to plants grown at optimum Ca^{2+} level (Fig. 1A). Plants were then dried at 65 °C overnight, and root and shoot dry matters were determined. As shown in Fig. 1B, Ca^{2+} deficiency decreases shoot and root biomass by 45% and 35%, respectively. The results also showed that prolonged low Ca^{2+} treatment decreased shoot and root elongation and plant height significantly from 66 to 38 cm, while root length was affected only slightly from about 15 cm to 12 cm (Fig. 1C).

Ca^{2+} deficiency disturbs minerals homeostasis. Fourteen-day-old seedlings were cultured in hydroponic solutions supplemented with 0.01 mM or 1 mM Ca^{2+} for one month. Mineral content from the dried shoot and root samples was determined using an inductively coupled plasma-optical emission spectrometer (ICP-OES). Plants grown in low Ca^{2+} media accumulated 0.5 g/Kg Ca^{2+} in the shoot (LCS) as compared to plants grown at optimum Ca^{2+} level (ConS), which accumulated 3 g/Kg Ca^{2+} (Fig. 2A). However, there was no statistically significant difference in root Ca^{2+} content. Similarly, there was no significant difference in root P content in plants grown at low (LCR) and optimum Ca^{2+} (ConR). At the same time, there was a small but statistically significant difference between LCS and ConR (Fig. 2B). S contents in root were slightly higher in plants grown at low Ca^{2+} while shoot S content was significantly lower in LCS than ConR (Fig. 2C). Ca^{2+} deficiency significantly suppressed root and shoot K content (Fig. 2D). In roots, K content decreased from 24.2 g/Kg in control plants to 10.3 g/Kg in Ca^{2+} deficient plants. Similarly, shoot K content decreased from 52.9 g/Kg in control plants to 32.2 g/Kg in Ca^{2+} deficient plants, suggesting the role of Ca^{2+} in K^+ uptake and homeostasis. Ca^{2+} deficiency also decreased Mg content in the roots, but it did not affect shoot Mg content (Fig. 2E). Interestingly, Fe content in LCR was 2.5-fold higher than ConR, 0.95 g/Kg and 0.36 g/Kg, respectively (Fig. 2F). However, Fe content in

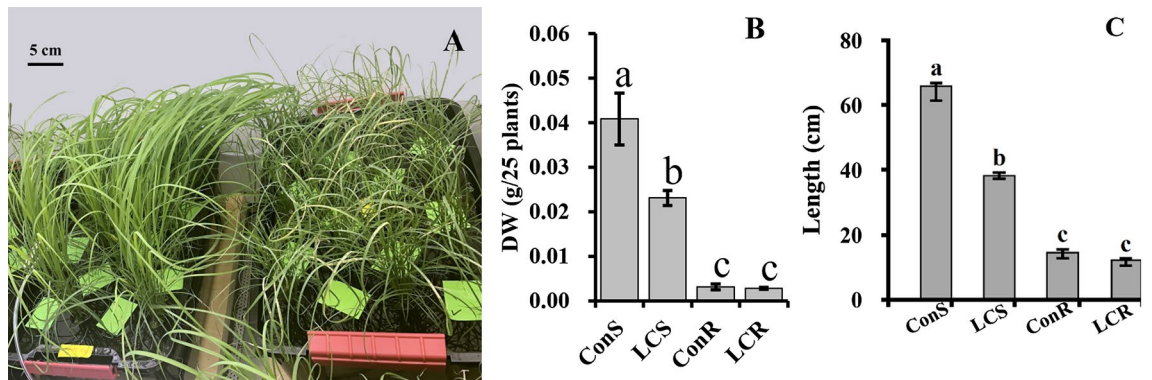


Figure 1. The phenotypic response of tef (*Eragrostis tef*) plants to long-term Ca treatment. (A) Phenotypes of tef plants treated with low (10 μ M) or optimum or control (1 mM) calcium in modified Hogland’s hydroponics media for four weeks. The picture was taken using an Apple iPhone camera by AL-O. (B) Root and shoot biomass, and root length of tef plants grown in Hoagland solution containing 10 μ M or 1 mM Ca. LCS, low calcium grown shoots; ConS, control/optimum Ca grown shoots. LCR, low calcium grown roots; ConR, optimum calcium treated roots. (C) Shoot and root length of tef plants grown under control (ConS and ConR) and low Ca (LCS and LCR) conditions. Bars represent mean and SD of at least 4 independent biological replicates, and different letters indicate statistically significant difference ($p < 0.05$).

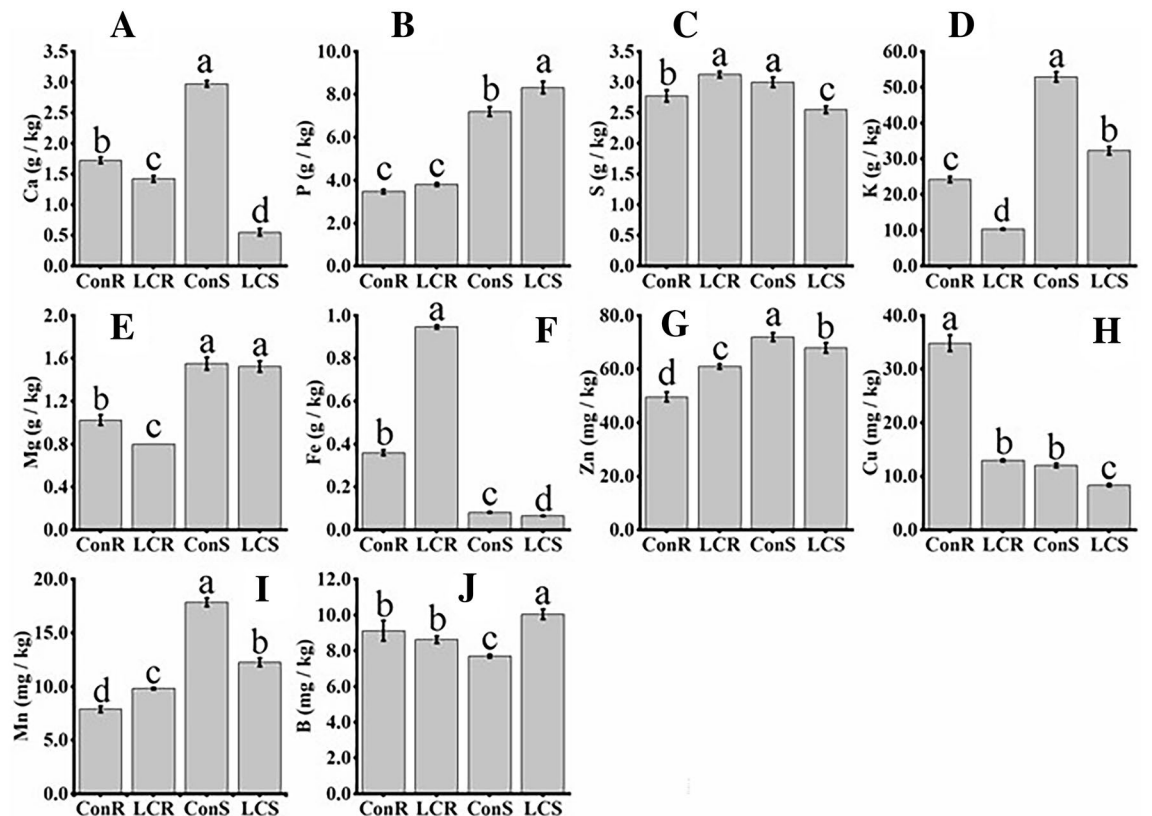


Figure 2. Mineral content profiling of tef plants grown under low or optimum Ca conditions. Shoot and root Ca (A), P (B), S (C), K (D), Mg (E), Fe (F), Zn (G), Cu (H), Mn (I) and B (J) were analyzed using ICP-OES as described in the “Materials and methods” section. Bars represent mean and SD of at least 4 independent biological replicates, and different letters indicate statistically significant difference ($p < 0.05$).

LCS (0.06 g/Kg) was slightly lower than in control plants (0.08 g/Kg), suggesting that Ca^{+2} deficiency impairs root to shoot translocation of Fe. The Zn content was slightly higher in LCR as compared to ConR, while in shoots, Zn content was slightly lower in LCS than ConS (Fig. 2G). We also observed that Cu accumulation was significantly affected by Ca^{+2} treatment. Ca^{+2} deficiency decreased root Cu content by three-folds (from 0.04 g/kg in ConR to 0.013 g/Kg in LCS), while in shoots, a small but significant decrease in Cu content was observed (0.01 g/Kg in ConS to 0.01 g/kg in LCS) (Fig. 2H). Both zinc (Zn) and copper (Cu) contents were lower in shoots

Treatments	LCR	LCS	ConR	ConS
Number of input reads	22,769,930	25,179,862.3	36,184,172.5	34,989,385.3
Number of uniquely mapped reads	18,361,838.8	21,930,270.8	28,709,324.8	31,726,862.3
Percentage of uniquely mapped reads	80.7	86.9	84.5	90.7
Number of reads mapped to multiple loci	1,956,523.75	1,285,027	2,371,076.75	1,791,236.5
Unmapped reads (too short) percent	8.45	5.115	6.555	5.1175

Table 1. RNA sequencing profile of *tef* samples under two different Ca^{2+} levels in root and shoots. Samples were LCR (low calcium roots), LCS (low calcium shoots), ConR (control roots) and ConS (control shoots). Note that values are averages of reads from four biological replicates.

than in roots. The manganese (Mn) content in the roots was slightly higher in LCR than ConR, while Mn content was significantly lower in LCS as compared to ConS (Fig. 2I). B content in roots was not affected by Ca^{2+} treatment, whereas shoot B content was significantly higher in LCS than ConS (Fig. 2J). Taken together, Ca^{2+} deficiency markedly affects mineral homeostasis, primarily cations.

Characteristics of RNA sequencing data. Since Ca^{2+} deficiency-induced visual symptoms in *tef* plants, including growth stunting and leaf necrosis in *tef* (Fig. 1A), we aimed at analyzing genome-wide transcriptomic changes in response to Ca^{2+} treatment. Total RNA was isolated from control and low Ca^{2+} -grown shoots and roots (ConR, ConS, LCR, and LCS). Complementary DNA libraries were generated from four independent biological replicates and sequenced using the paired-end sequenced using Illumina HiSeq 4000. A total of 476.5 million raw reads with an average of 30 million reads were obtained for each sample. The total clean reads of the 16 libraries were aligned to the *tef* draft genome sequence³⁸. On average 85.7% of the reads were uniquely aligned to the reference genome (Tables 1, S1).

Analysis of differentially expressed genes (DEGs). The quality of sequence reads was assessed using fastqc application, and 15 poor-quality bases were trimmed from the 5'-end. The remaining good-quality reads were aligned to the *tef* reference genome using hisat2 aligner³⁹. For each replicate, per-gene counts of uniquely mapped reads were calculated using the htseq-count script from the HTSeq⁴⁰ python package. The count matrix was imported to R statistical computing environment for further analysis. Initially, genes that have no count in the replicate samples were discarded. The remaining count data were normalized and differentially expressed genes were identified using the DESeq2⁴¹ R package⁴².

To determine the integrity of RNA samples, we performed principal component analysis (PCA). The PCA shows no mark variation among most RNA samples from the same Ca^{2+} treatment or tissue (Supplementary Fig. 1A,B). Our analysis identified many DEGs in response to Ca^{2+} treatment suggesting the crucial role of Ca^{2+} in plant physiological processes, including overall plant performance (Fig. 1) and mineral homeostasis (Fig. 2). The Venn diagram in Fig. 3A summarizes the pairwise comparisons of different groups (LCR, LCS, ConR, and ConS) based on the number of DEGs regulated in roots and shoots of *tef* plants grown under low and optimum Ca^{2+} conditions. As compared to ConR, 824 DEGs were detected in LCR, of which 85 are unique to LCR. A total of 5,420 DEGs out of 28,796 genes were detected in LCS as compared to ConS of which 531 DEGs were uniquely detected in LCS. Relative to LCS, 10,752 DEGs were seen in LCR of which 532 DEGs are unique to LCR. A total of 13,504 DEGs were detected in ConR as compared to LCR, of which 1,886 DEGs were uniquely detected in ConR. A total of 249 DEGs were common in all the pairwise comparisons (LCR vs. ConR, LCS vs. ConS, LCR vs. LCS, and ConR vs. ConS).

Figure 3B illustrates the transcriptomic response of *tef* plants grown in optimum and low Ca^{2+} conditions. A large number of genes (4,654) were upregulated in roots and shoots of low Ca^{2+} relative to control, of which 366 and 4009 genes were uniquely upregulated in LCR and LCS relative to ConR and ConS, respectively. A total of 279 genes were commonly upregulated in LCR and LCS. We also detected 1279 DEGs that were downregulated in LCR (179) and LCS (1132) compared to ConR and ConS, respectively. A total of 32 genes were commonly downregulated in LCR and LCS as compared to ConR and ConS, respectively. Ca^{2+} deficiency also induced significant transcriptomic changes between roots and shoots. A total of 7045 DEGs were upregulated in roots, of which 4833 DEGs were upregulated in LCR relative to LCS, 6670 DEGs were upregulated in ConR relative to ConS, and 4458 DEGs were commonly upregulated in both LCR and ConR. Similarly, 7430 DEGs were downregulated in roots, of which 6,192 DEGs were downregulated in LCR relative to LCS, 6834 DEGs were downregulated in ConR relative to ConS, and 5596 DEGs were commonly downregulated in both LCR and ConR relative to LCS and ConS, respectively. Taken together, the number of transcripts that were upregulated in response to Ca^{2+} deficiency in both roots and shoots were higher than those whose transcript abundance was downregulated. Moreover, the number of DEGs that were upregulated in ConR versus ConS were higher than those DEGs that were upregulated in LCR versus LCS (Fig. 3B).

GO annotation of DEGs. We performed Gene Ontology (GO) enrichment analysis using the AgriGo database to determine the potential function of DEGs identified in our analysis. In the GO analysis, the DEGs were grouped into molecular function, cellular components, and biological process categories (Fig. 4). Of these categories, DEGs with catalytic activity (>1300 DEGs) were the most highly enriched group (Fig. 4A) for the

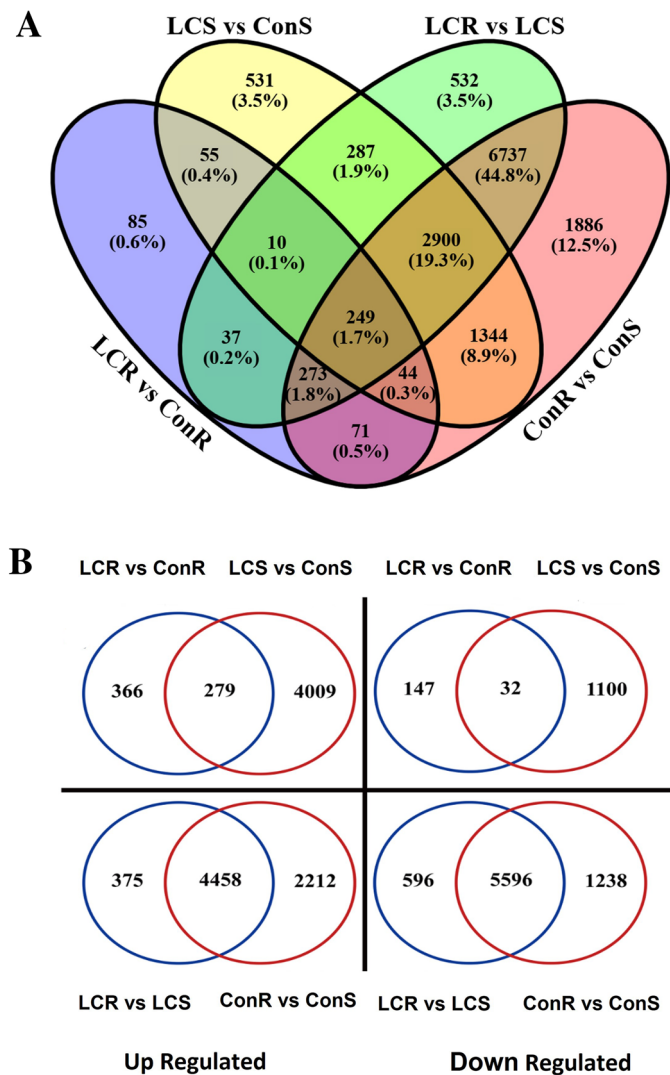


Figure 3. Transcriptomic response of *tef* in response to Ca^{2+} treatment. (A) Venn diagram illustrating the number of DEGs between the two Ca^{2+} treatment groups in root and shoot tissues, and (B) Venn diagram illustrating the number of differentially expressed genes between different treatment group. The treatment groups are LCR versus ConR, LCS versus ConS, LCR versus LCS and ConR versus ConS.

LCR vs ConR comparison, followed by those predicted to have transport activity (200 DEGs). In the cellular component category, all the DEGs that were enriched are associated with membranes. In contrast, in the biological process category, about 300 DEGs are predicted to be involved in establishing localization, transport, and transmembrane transport. We also noted that DEGs with metal ion transporter activity, ATPase activity, primary active transporter activity, inorganic cation transporter activity, and substrate-specific transporter activity were on top of the list (Fig. 4A). When LCS versus ConS comparison was used for GO analysis, we observed that DEGs with hydrolase activity, ATP binding, and kinase activity were most enriched in the molecular function category. In contrast, in the biological process category, genes with cellular process followed by the primary metabolic process is the most enriched group (Fig. 4B).

Calcium transporter genes are differentially regulated in response to Ca^{2+} treatment. Several families of genes have been implicated in Ca^{2+} transport in plants. This study identified transcriptomic changes in some families of Ca^{2+} transporters, including GLRs, CNGCs, Ca^{2+} uniporters, cations/ Ca^{2+} exchangers, and Ca^{2+} -transporting ATPases. Our analysis identified Ca^{2+} transporters including Ca^{2+} uniporters, cation/ Ca^{2+} exchangers and Ca^{2+} transporting ATPase (Fig. 5A) etc. Expression of putative Ca^{2+} uniporters *CaUP2* and *CaUP4* were higher in roots than shoots in both low and optimum Ca^{2+} conditions. Transcripts of several transporters, including *CaE1-1*, *CaTA5-1*, *CaTA9-1*, *CaUP6*, *CaUP3*, *NaCaE1* were more abundant in ConS relative to ConR while transcripts of *CaE1-2*, *CaUP3*, *CaTA3*, and *CaUP4* were more abundant in LCR than LCS. Transcripts of *CaE1* was more abundant in LCS than ConS, while *CaTA9*, *CaTA5-1*, *CaTA9-1*, *CaUP6*, and *CaTA10* were more abundant in ConS than LCS. *CaE1*, *CaE1-1*, and *CaUP4* are more abundant in LCR than ConR,

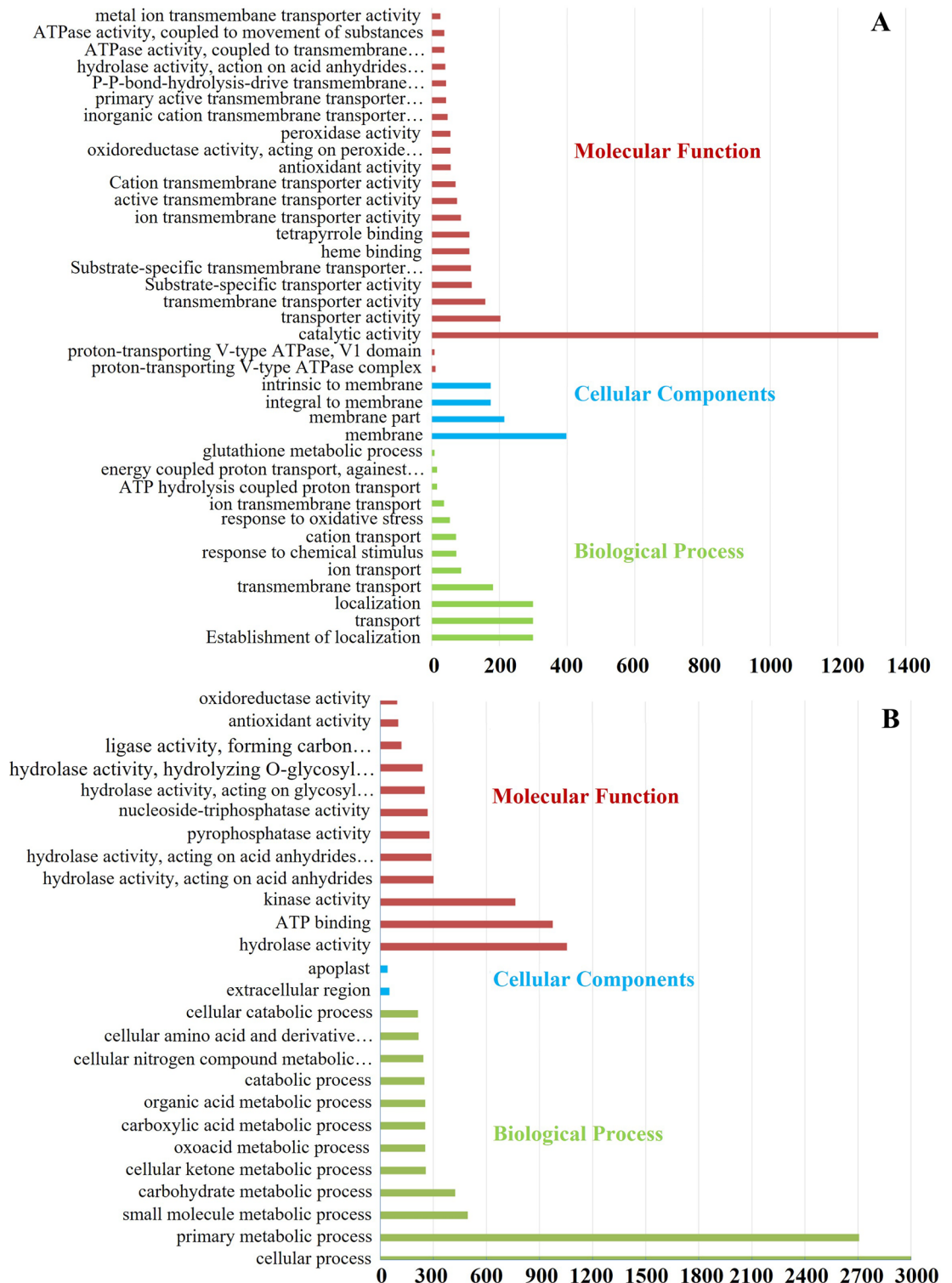


Figure 4. Gene Ontology (GO) enrichment terms of DEGs. Bars represent the number of genes enriched in LCR versus ConR (A), and the number of genes enriched in LCS versus LCS (B). GO annotation was performed as described in the “Materials and methods” section.

whereas CaTA5 is more abundant in ConR than LCR. Transcripts of several members of Ca²⁺ transporting proteins are not markedly affected by Ca²⁺ treatment and between roots and shoots (Fig. 5A).

In response to Ca²⁺ treatment, several Ca²⁺-binding, Ca²⁺ signaling, and other transporters, including Ca²⁺ transporters and Ca²⁺-gated channels, are differentially expressed in both roots and shoots. We analyzed the expression of the CNGCs, which are implicated in the transport of Ca²⁺ and other cations (Fig. 5B). Transcripts of *CNGC2*, *CNGC4*, *CNGC4.1*, and *CNGC4.2* were more abundant in shoots than roots under low and optimum

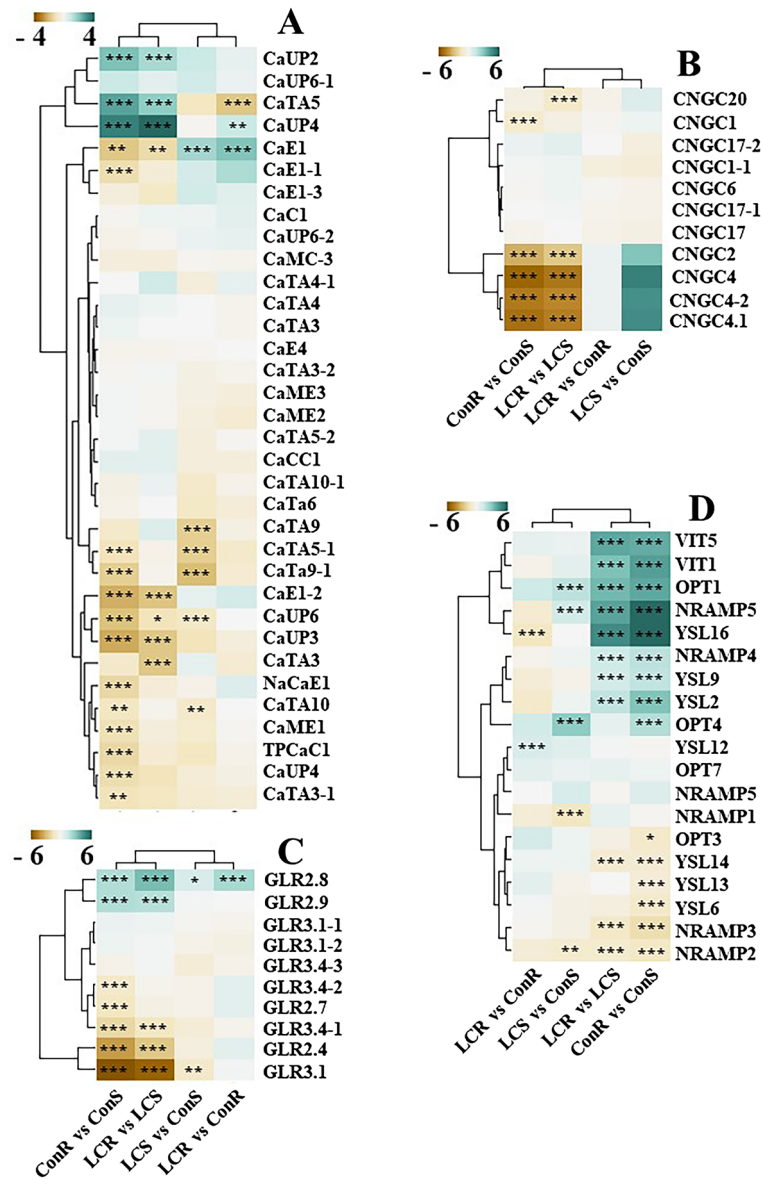


Figure 5. Heatmaps of differentially expressed genes. (A) Calcium transporters, (B) CNGCs, (C) GLRs and (D) Fe/metal transporters. Fe, iron; GLR, glutamate receptor; CNGC, cyclic nucleotide-gated channel; OPT, oligopeptide transporter; VIT, vacuolar iron transporter; NRAMP, metal transporter Nramp; YSL, yellow stripe-like; CaC1, calcium load-activated calcium channel; CaCC1, calcium permeable stress-gated cation channel 1; CaUP, calcium uniporter protein; CaMC, calcium-binding mitochondrial carrier protein; CaTA, calcium-transporting ATPase; CaE, cation/calcium exchanger; CaME, mitochondrial proton/calcium exchanger protein; NaCaE, sodium/calcium exchanger; TPCaC, two pore calcium channel protein. * $p < 0.05$; ** $p < 0.01$; *** $p < 0.001$. (A) Et_4A_032234, CaC1; Et_3B_028475, CaCC1; Et_1A_007032, CaUP2; Et_4A_035795, CaUP4; Et_3B_029644, CaUP6; Et_10A_001249, CaUP6-1; Et_6A_048187, CaUP6-2; Et_1A_008615, CaUP3; Et_7B_055244, CaUP4; Et_2B_021219, CaMC-3; Et_4B_039870, CaTA10; Et_10B_003581, CaTA10-1; Et_4A_033710, CaTA3; Et_4B_037342, CaTA3-1; Et_4A_033168, CaTA3-2; Et_4A_034993, CaTA4; Et_9A_061403, CaTA4-1; Et_1A_007426, CaTA5; Et_8A_057406, CaTA5-1; Et_8A_057411, CaTA5-2; Et_7B_054771, CaTA3; Et_10A_001931, CaE1; Et_1A_006089, CaE1-1; Et_4A_035362, CaE1-2; Et_1B_010978, CaE1-3; Et_4A_035689, CaE4; Et_7A_050701, CaME1; Et_1B_014429, CaME2; Et_9A_061952, CaME3; Et_9A_062174, CaTA6; Et_10A_001147, CaTA9; Et_6A_046490, CaTA9-1; Et_3A_023829, NaCaE1; Et_3A_024662, TPCaC1. (B) Et_1B_013097, OPT4; Et_1A_008454, YSL2; Et_1B_013348, YSL14; Et_2B_020454, VIT1; Et_2B_020954, Nramp3; Et_3B_028366, Nramp4; Et_3B_031448, YSL16; Et_4A_033828, OPT3; Et_4A_034655, Nramp2; Et_5A_041073, Nramp1; Et_5A_041086, Nramp5; Et_7A_051270, YSL6; Et_7A_052425, YSL9; Et_7B_055732, VIT5; Et_7A_053172, YSL13; Et_7B_055138, YSL12; Et_8A_058302, OPT1; Et_10B_003591, Nramp6; Et_2A_017928, OPT7. (C) Et_1A_006195, GLR2.7; Et_2A_016261, GLR2.4; Et_2A_016906, GLR3.4-1; Et_2A_018314, GLR2.9; Et_2A_018316, GLR2.8; Et_5B_043951, GLR3.4-2; Et_7A_052266, GLR3.1; Et_7B_054916, GLR3.1-1; Et_1A_008007, GLR3.1-2; Et_5B_045010, GLR3.4-3. (D) Et_1A_006672, CNGC20; Et_2A_016805, CNGC1; Et_3B_029538, CNGC4; Et_4B_038004, CNGC2; Et_4B_037294, CNGC4-1; Et_9B_064738, CNGC4-2; Et_1A_006188, CNGC17; Et_1A_007771, CNGC1-1; Et_2A_015772, CNGC17-1; Et_2A_017586, CNGC17-20; Et_7B_054569, CNGC6. The graphs were generated using R Software⁴²(URL <https://www.R-project.org/>).

Ca²⁺ conditions (Fig. 5B). The transcripts of these genes were more abundant in LCS than ConS, although not statistically significant. Expression of *CNGC1* and *CNGC20* are significantly downregulated in ConR and LCR as compared to ConS and LCS, respectively. There was no difference in the expression of CNGCs between LCR and ConS.

Figure 5 also shows that several putative tef glutamate receptors such as *GLR3.1*, *GLR2.8*, *GLR4-1*, and *GLR3.4-1* are differentially expressed in response to Ca²⁺ deficiency, as shown in Fig. 5C. In ConS, transcripts of *GLR2.4*, *GLR2.7*, *GLR3.1*, *GLR3.4*, and *GLR3.4-1* were more abundant than ConR, while *GLR2.4*, *GLR3.1*, and *GLR3.4-1* were more abundant in LCS than LCR. However, the transcripts of *GLR2.8* were more abundant in LCR than ConR.

Low calcium regulates the expression of Fe and metal transporter genes. Our analysis also revealed that several members of the putative iron transporters are differentially regulated in response to Ca²⁺ treatment and between tissue types (Fig. 5D). Transcripts of several tef homologs of *Arabidopsis* and rice iron transporter, including *VIT5*, *VIT1*, *OPT1*, *NRMAP5*, *YSL16*, *NRAMP4*, *YSL9*, and *YSL2* were more abundant in LCS and ConS than LCR and ConR, respectively. *YSL2* is a critical enzyme in long-distance Fe transport through the xylem. The VITs transport Fe across the vacuolar membrane, and Nramps and OPTs are involved in Fe other metal transport. The expression of *YSL14*, *NRAMP2*, and *NRAMP3* was downregulated under low Ca²⁺ conditions in both roots and shoots. Transcripts of *YSL13* and *YSL6* were more abundant in ConR than LCR. Transcripts of *OPT1*, *OPT4*, and *NRAMP5* were upregulated in LCR relative to LCS, while *NRAMP1* and *NRAMP2* were more abundant in LCS than LCR. Transcripts of *YSL16* is upregulated in ConS than ConR, while *YSL12* is upregulated in ConR than ConS (Fig. 5B).

Calcium signaling genes are differentially regulated by long-term Ca²⁺ treatment. Because Ca²⁺ plays a key role in various abiotic stress signaling, we analyzed whether transcripts of signaling genes respond to long-term Ca²⁺ deficiency. As shown in Fig. 6, many signaling genes, including CBP and CDPKs differentially regulated by Ca²⁺ treatment and between root and shoots. Transcripts of several genes, including *CDPK4*, *CBP6*, *CBP16*, and *CBP17*, are more abundant in shoots than roots under both Ca²⁺ levels. At the same time, transcripts of several CDPK and CBP, including *CDPK1*, *CDPK2*, *CDPK12*, *CDPK3*, and *CBP15*, were more abundant in the roots of both control and low Ca²⁺ conditions. In roots, the expression of *CDPK1*, *CDPK2*, *CDPK3*, *CCDSTK1*, and *CBP15*, is upregulated by Ca²⁺ deficiency. Overall, our findings highlight the differential expression of some signaling genes in response to long-term Ca²⁺ deficiency.

Validation of RNA-seq DEGs. To the RNA-seq data, we performed quantitative RT-PCR (qPCR) to analyze the expression of a few DEGs, including *CaE1*, *CGC2*, *GLR3.1*, and *CNGC17*. As shown in Fig. 7, we performed Pearson correlation of Log² fold changes in gene expression by RNA-seq and qPCR analysis. A strong positive correlation was observed between the two assays for *CaE1* (R²=0.9167), *CNGC2* (R²=0.9626) and *CaE1* (R²=0.9626), while a positive but weak correlation was observed for *CNGC17* (R²=0.1689). These findings validate the RNA-seq data.

Discussion

The Chloridoideae subfamily of Poaceae, including tef and finger millet, accumulate higher levels of Ca²⁺ in grains than other cereals⁴³. However, the effect of prolonged Ca²⁺ deficiency on their physiology and transcriptome remained unknown. In the present study, we examined the response of tef to prolonged Ca²⁺ deficiency based on agronomic, physiological, and transcriptome changes in plants grown in hydroponics solution under optimum and Ca²⁺ deficient conditions.

Tef plants grown under Ca²⁺ deficient conditions showed typical deficiency symptoms in shoots, including leaf curling, tip necrosis, and growth stunting (Fig. 1A), which is in line with previous reports⁴⁴. We performed the elemental analysis of the shoots and roots to validate our phenotypic analysis. Our findings revealed that prolonged Ca²⁺ deficiency significantly decreased Ca²⁺, K, and Cu content in both the roots and the shoots, and S, Zn, and Mn in the shoots. Interestingly, Fe translocation from roots to shoots is significantly suppressed by Ca²⁺ deficiency. Root Fe content was 2.5-fold higher in roots than in shoots. These suggest that Ca²⁺ deficiency suppresses plant growth by perturbing homeostasis of essential minerals, including macro and micronutrients. Ca²⁺ deficiency is rare in nature but may happen when plants are grown in acidic soil⁴. Although there is no report on the effect of Ca²⁺ deficiency on plant Fe translocation, some studies have reported on the interaction between Ca²⁺ and Fe. A high level of Ca²⁺ has been reported to cause Fe chlorosis by suppressing Fe acquisition in field crops⁴⁵ and decreased Fe uptake in dry bean plants⁴⁶.

To understand the transcriptomic change in response to Ca²⁺ deficiency, we performed RNA-seq using the Illumina HiSeq platform. Our analysis revealed that many transcripts are differentially regulated between control and Ca²⁺ deficient conditions, and between roots and shoots of plants grown under both Ca²⁺ treatments (Figs. 3 and 5). Moreover, our GO analysis highlighted significant enrichment of several Ca²⁺ transporters, signaling genes, those genes with transport activities, ATPase activity, catalytic activities etc. (Fig. 5). Such transcriptomic changes are expected since Ca²⁺ is an integral part of plant cell walls, mineral homeostasis, and signaling⁴⁴.

When plants undergo certain environmental stresses, Ca²⁺ signals are generated, which trigger a rapid rise in cytosolic Ca²⁺ levels⁴⁷. Several protein families are implicated in plants' Ca²⁺ transport processes, including Ca²⁺-permeable ion channels, Ca²⁺/H⁺ exchangers, and pumps (Ca²⁺-ATPases)¹. Several Ca²⁺-permeable channels have been implicated in the uptake of Ca²⁺ from the soil solution to plant roots⁴⁸. These include the GLRs, CNGCs, two-pore channels (TPCs), mechanosensitive-like channels (MSLs) etc.⁴⁹. Ca²⁺ pumps are involved in maintaining homeostasis by controlling Ca²⁺ efflux from the cytosol to organelles and/or to the apoplast⁵⁰.

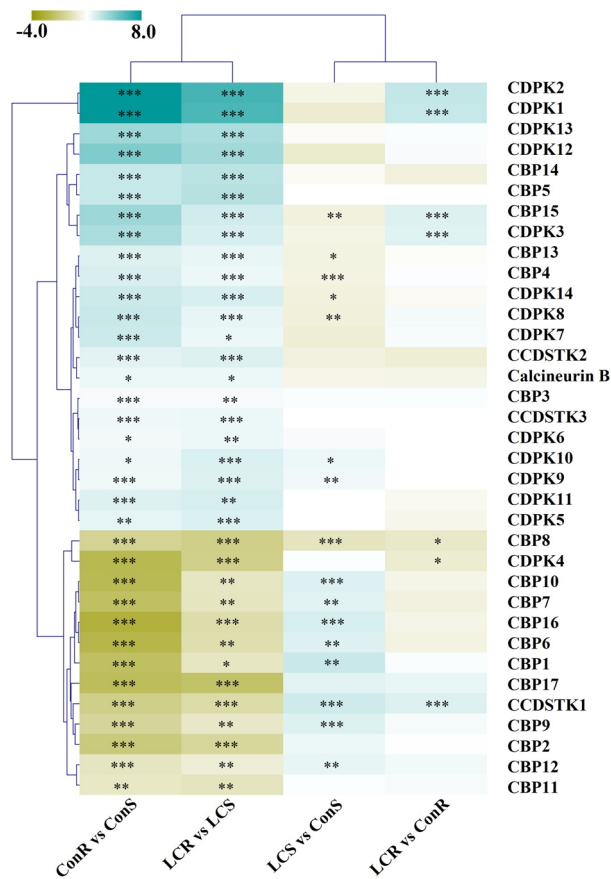


Figure 6. Heatmap of differentially expressed Ca^{2+} -signaling genes. Several families of Ca^{2+} -signaling genes are differentially regulated between the Ca treatment and root and shoot tissues. CCDSTK, calcium/calmodulin-dependent_serine/threonine-protein_kinase; CBP, calcium-binding_protein; CDPK, calcium-dependent_protein_kinase. Et_8B_060076, Calcineurin B; Et_4B_036878 CCDSTK1; Et_5A_041770, CCDSTK2; Et_5B_044444, CCDSTK3; Et_1B_010286, CBP1; Et_1B_014273, CBP2; Et_9A_062108, CDPK1; Et_9B_064669, CDPK2; Et_4A_033992, CDPK3; Et_7A_052314, CDPK4; Et_7B_054972, CDPK5; Et_2A_018014, CDPK6; Et_5A_040958, CDPK7; Et_5B_043654, CDPK8; Et_10A_000985, CDPK9; Et_10B_003165, CDPK10; Et_1A_008319, CDPK11; Et_4A_032792, CDPK12; Et_4B_036955, CDPK13; Et_5B_045743, CDPK14; Et_9A_063197, CBP3; Et_5B_044570, CBP4; Et_3A_023309, CBP5; Et_9B_066197, CBP6; Et_2B_022523, CBP7; Et_2A_018508, CBP8; Et_6A_046999, CBP9; Et_6B_049755, CBP10; Et_3A_023424, CBP11; Et_3B_027891, CBP12; Et_8A_057679, CBP13; Et_10A_001142, CBP14; Et_10B_004199, CBP15; Et_2A_017214, CBP16; Et_2B_021205, CBP17. The graph was generated using R Software⁴²(URL: <https://www.R-project.org/>).

In our dataset, we identified several DEGs including Ca^{2+} uniporters (CaUPs), cation/ Ca^{2+} exchangers (CaE), Ca^{2+} -transporting ATPases (CaTA) etc. (Fig. 5). Our findings revealed that that the *CaE1-1*, *CaTA5-1*, *CaTa9-1*, *CaE1-2*, *CaUP6*, *CaUP3*, *NaCaE1*, *CaTA10*, *CaME1*, *TPCaC1*, *CaUP4* and *CaTA3-1* were downregulated in ConR as compared to ConS (Fig. 5A). Whereas CaE1, CaE1-2, CaUP3, and CaTA3 were downregulated in LCR compared to LCS (Fig. 5A). When the LCS was compared to ConS, the *CaE1* was upregulated, and *CaTA9*, *CaTA5-1*, *CaTA9-1*, *CaUP6*, and *CaTA10* were downregulated. Similarly, when LCR was compared with ConR, the CaUP4 and CaE1 genes were upregulated, and *CaTA5* was downregulated (Fig. 5A). For example, *CaUP2*, *CaTA5*, and *CaUP4* were more highly expressed in ConR and LCR than ConS and LCS, respectively (Fig. 5A). It was previously reported that Ca^{2+} uniporters play an important role in stress signaling in Arabidopsis⁵¹. In another study, Ca^{2+} uniporter proteins were implicated in pollen tube germination⁵². As reported in previous studies, Ca^{2+} uniporters play an important role in Ca^{2+} signaling and homeostasis in Arabidopsis⁵¹ and homologs in mammals play role in Ca^{2+} uptake into the mitochondrial matrix and regulate calcium signaling, aerobic metabolism, and apoptosis⁵³. None of these transporters have been isolated and characterized from tef before. However, several homologs have been characterized in other plant species such as Arabidopsis⁵⁴, rice⁵⁵ and apple (*Malus domestica*)⁵⁶.

The CaCA superfamily has been reported to facilitate Ca^{2+} transport against its concentration gradient and enhance the influx of monovalent cations (K^+ , Na^+ , and H^+)⁵⁷. For example, overexpression of the apple cation/ Ca^{2+} exchanger MdCCX1 in transgenic Arabidopsis and apple root cells has been shown to decrease Na^+ accumulation and ROS levels and increase salt tolerance in transgenic cells⁵⁶. In this study, Ca^{2+} deficiency decreased

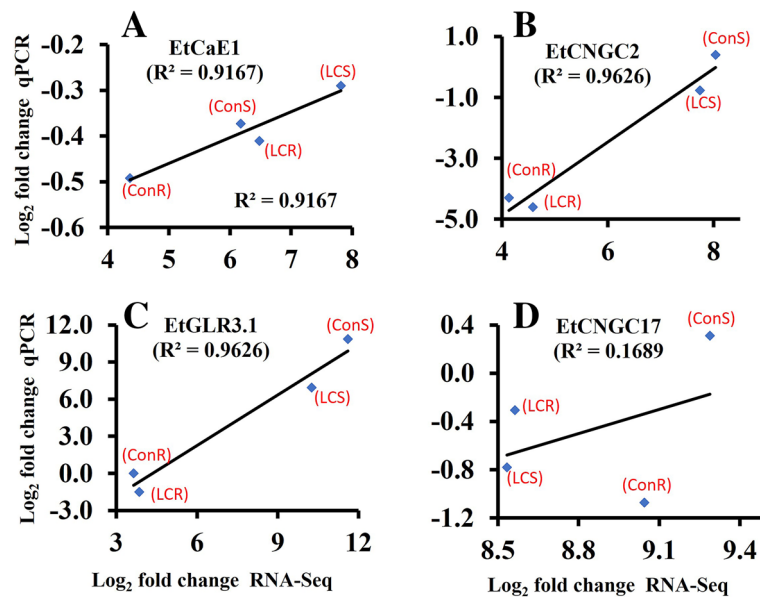


Figure 7. Validation of RNA-seq data by qPCR. Pearson correlation analysis of Log₂ fold changes of DEGs based on RNA-seq and qPCR analysis. Data points and corresponding treatments (ConR, ConS, LCR and LCS) are shown.

Ca and K content in roots. Therefore, upregulation of CaE1 in LCR and LCS could be a mechanism by which roots enhance K⁺ or Ca²⁺ acquisition from the external solution or facilitate their distribution between tissues. Transcripts of *CaTA9-1*, *CaTA5-1*, *CATA9*, and *CaUP6* are downregulated by Ca²⁺ deficiency in the shoots. The *CaTA5* was the only gene among the transporters that was downregulated by Ca²⁺ deficiency in roots. *CaTA5* is a homolog of the plasma membrane Ca²⁺-transporting ATPases (PMCA), which are high-affinity Ca²⁺-pumps that export Ca²⁺ ions from the cytosol into the extracellular solution⁵⁸. *CaTA5* may be a functional Ca²⁺-pump, and its downregulation under Ca²⁺ deficiency could be a strategy to suppress the cytosolic Ca²⁺ export to the extracellular solution. The autoinhibited Ca²⁺-ATPase *ACA13* has been implicated in successful pollination in the *Brassicaceae* by exporting pollen to compatible pollen tubes⁵⁹.

This study also identified various Fe/metal transporters, including OPTs, VITs, NRAMPs, and YSLs. All these transporters proteins were differentially expressed in the roots and shoots of low Ca²⁺ and control plants. In Arabidopsis, *Oligopeptide Transporter 1* (*AtOPT1*) is a major nitrate/oligopeptide transporter family⁶⁰. The Arabidopsis *OPT3* is a phloem-specific iron transporter⁶¹ and its rice counterpart, *OsOPT7*, has been implicated in Fe loading into the phloem, the long-distance Fe transport, and loading to seeds^{62,63}. *OPT4* is involved in oligopeptide transport⁶⁴. Furthermore, Arabidopsis *Oligopeptide Transporter 6* (*AtOPT6*) was reported to transport glutathione⁶⁵ and a possible connection between prolonged Ca²⁺ deficiency, redox status, and increased iron transport is a likely scenario as suggested in a recent review²⁸. In this study, transcript levels of several transporters such as *OPT1*, *EtNRAMP5*, *EtVIT5* and *EtYSL2* were upregulated by several folds (Fig. 5B) in the shoot during Ca²⁺ deficiency. Similarly, the *VIT1*, *YSL16*, *NRAMP4*, *YSL9* and *OPT4* were upregulated in both LCR vs. LCS and ConR vs. ConS. The transcripts of *OPT1*, *NRAMP5*, and *OPT4* were also upregulated, while that of *NRAMP1* and *NRAMP2* were downregulated in the LCR compared to ConR (Fig. 5D). The maize *ZmYSL1*⁶⁶ and rice *OsYSL15*⁶⁷ import Fe³⁺-phytosiderophore (PS) across the root cell membrane, while the rice *OsYSL2* is implicated in the long-distance transport of Fe associated with a PS precursor, nicotianamine (NA)⁶⁸. The role of *YSL2* in Fe uptake and distribution has been studied previously in maize⁶⁹ and Arabidopsis^{70,71}. The NRAMPs such as *AtNRAMP3* and *AtNRAMP4* function in transporting Fe out of vacuoles under Fe-limited conditions, while members of the VIT family mediate Fe transport into vacuoles⁷². For example, overexpression of the wheat *VIT2* under the control of an endosperm-specific promoter increases Fe content in white flour fractions of wheat⁷³. Some of these transporters are not specific to Fe but also transport other minerals, including Zn, Cd, Cu, and Mn⁷⁴. Taken together, differential regulation of several mineral transporters in response to Ca nutrition suggests the involvement of Ca²⁺-signaling in the homeostasis of these minerals. The decrease in root to shoot Fe translocation in this study due to Ca²⁺ deficiency (Fig. 2F) suggests the involvement of Ca²⁺ signaling in Fe homeostasis. Ca²⁺-signaling has been implicated in the homeostasis of minerals such as K⁺. In this regard, Gratz et al.⁷⁵ reported that CIPK11-dependent phosphorylation modulates the activity of FIT (a transcription factor that regulates Fe acquisition), promoting Fe uptake in Arabidopsis. Ca²⁺ promotes the interaction of C2-Domain Protein Enhanced Bending1 (EHB1) and the root Fe-regulated transporter IRT1, inhibiting Fe acquisition in Arabidopsis⁷⁶. However, further studies are needed to understand the crosstalk between Fe and Ca nutrition in Ca and Fe-rich cereals such as teff and finger millet.

Our study also revealed that several Ca²⁺-transporting channels were differentially expressed by Ca treatment. Our findings showed that transcripts of the CNGC, including *CNGC2*, *CNGC4*, and *CNGC4-2*, were more abundant in the shoots regardless of the Ca treatment (Fig. 5B). This may suggest that the CNGC may be involved

in Ca^{2+} distributions in the shoots. The CNGC has lower ion selectivity permeating K^+ , Na^+ and Ca^{2+} across the plasma membrane. The Arabidopsis genome consists of 20 members of the CNGC, and all the CNGC tested so far transport K^+ , while some members of the CNGC also translocate Ca^{2+} ⁷⁷. The Arabidopsis CNGC2 and CNGC4 are implicated in pathogen-induced Ca^{2+} -signaling⁷⁸. The CNGC2 and CNGC4 have also been implicated in plasma membrane external ATP-activated Ca^{2+} influx in pollen tubes of Arabidopsis⁷⁹. As shown in Fig. 5C, *GLR2.8* and *GLR2.9* were significantly upregulated in ConR compared to ConS while *GLR3.4-2*, *GLR2.7*, *GLR3.4-1*, *GLR2.4* and *GLR3.1* were downregulated. Similarly, *GLR2.8* and *GLR2.9* were upregulated in LCR compared to LCS, while *GLR3.4-1*, *GLR2.4*, and *GLR3.1* were downregulated. In Arabidopsis, the GLRs such as GLR 3.1, GLR 3.2, and GLR 3.3 GLR 3.6 have been reported to mediate long-distance Ca^{2+} signaling during wound responses¹⁰. Heterologous expression of the rice OsGLR2.1 in mammalian cells resulted in Glu-triggered Ca^{2+} increase³⁰. Similarly, in the basal land plant mosses (*Physcomitrella patens*)⁹, it has been shown that GLR1 encodes a non-selective ion channel that is permeable to Ca^{2+} . Upregulation of *GLR2.8* and *GLR2.9* in roots compared to shoots in this study may suggest their involvement in Ca^{2+} uptake in the roots. Upregulation of *GLR2.8* in LCR compared to ConR may suggest its role in Ca^{2+} acquisition under Ca^{2+} -deficient conditions. However, the GLRs which were upregulated in the shoots under both high and low Ca^{2+} , such as *GLR3.4-1*, *GLR2.4*, and *GLR3.1*, may play a role in Ca^{2+} distribution in the shoots, which remains to be studied in the future.

In conclusion, we found that Ca^{2+} deficiency severely inhibits the growth of tef plants by disturbing the homeostasis of some minerals, including Ca, K, Fe, Mn, and Cu. Furthermore, our transcriptomic analysis revealed various genes, including those implicated in Ca^{2+} -signaling, Ca^{2+} -transporters, and Ca^{2+} -permeable channels; Fe and metal transports which were differentially regulated by Ca^{2+} deficiency and/or between root and shoot tissues, suggesting their involvement in Ca^{2+} homeostasis. Heterologous expression and loss-of-function mutations studies of the DEGs identified in this study would elucidate their physiological functions in tef.

Materials and methods

Plant materials and growth condition: We recently performed seed mineral profiling of diverse tef (*Eragrostis tef*) accessions obtained from the USDA-GRIN germplasm collection⁴³. We used the accession with the highest seed Ca (1811 mg/kg) content in this study. Tef seeds were sterilized according to a method previously published with slight modifications⁸⁰. Briefly, seeds were soaked in 70% ethanol for one minute, followed by soaking in 1% NaOCl solution containing 0.1% Tween-20 for 10 min with vortexing every 1 min. Subsequently, the seeds were washed with autoclaved high purity water (18.2 M Ω (megaohms)) five times. The seeds were then transferred to a petri-dish with a sterile wet filter paper disc. The plates were incubated in a growth chamber (Conviroon, Winnipeg, Canada) for six days under 16 h/8 h day-night cycles at 28 °C. The seedlings were transferred to a modified Hoagland hydroponic solution⁸¹ in which the $\text{Ca}(\text{NO}_3)_2$ was replaced with NH_4NO_3 to investigate the effect of Ca^{2+} . Plants were grown in the media containing either 1 mM Ca^{2+} (optimum or control) or 10 μM (low Ca or Ca-deficient). The nutrient solution was continuously aerated and was renewed every 4 days.

Plant phenotyping/photography. Images were taken from the plants grown in a hydroponics system after ~28 days. Root and shoot dry weight biomass were measured at the end of the prolonged Ca^{2+} deficiency treatment. The measurements were taken for all replicates and mean values were calculated.

Mineral element analysis. One-month-old tef plants grown in 1/4th-strength Hoagland's hydroponics solution was analyzed. Roots and shoots were separated and rinsed three times with Milli-Q (18.2 M Ω) water. Before weight measurements, the tissues were oven dried at 65 °C overnight and ground to fine powder using a Waring Laboratory spice blender. Briefly, 500 mg of ground tissue was digested using concentrated HNO_3 for 30 min in a microwave at 200 °C, and mineral content was analyzed using Inductively Coupled Plasma Optical Emission Spectroscopy (ICP-OES).

Library construction and RNA sequencing. For RNA extraction, root and shoot samples were ground into powder under liquid nitrogen using a mortar and pestle. Total RNA was isolated using the GeneJET RNA purification kit following manufacturer's procedure (Thermo Fisher Sci., Waltham, MA). The quality and quantity of the RNA were determined using a Nanodrop (Thermo Fisher Sci, Waltham, MA). mRNA-seq libraries were prepared using NEBNext® Ultra II RNA Library Prep Kit for Illumina (New England Biolab EB, Ipswich, MA) according to the manufacturer's instructions. For each library, 500 ng total RNA was used. The mRNA-seq libraries were sequenced on an Illumina HiSeq platform using the 150 bp paired-end sequencing strategy.

RNA-seq data analysis. Data analysis for RNA-Seq was performed by the Bioinformatics Core associated with the Center for Human Health and Environment at North Carolina State University. Quality control of read data was briefly evaluated with FastQC, and alignment trimming was performed using *sickle* with the options -q 12 and -l 15 (version 1.33⁸²). Alignment was performed using *hisat2* short read aligner to Tef reference genome downloaded from CoGe Comparative Genomics website (V3.1, id59854)³⁸. All default parameters were used except -very-sensitive and -summary-file options passed to the *hisat2* aligner⁸³. The number of reads mapped to a genome feature was determined using *htseq-count* command line script from the HTSeq python package⁸⁴ (-s reverse -a 10 -t exon -I Parent -m union) and count data was imported to the R statistical computing environment for further analysis⁴². Initially, genes that have no count in at least 4 of the replicate samples were excluded from the analysis, and the remaining 28,796 features were used for downstream analysis. Data normalization based on dispersion and differential analysis were conducted using the DESeq2 package⁸⁵. We fitted a generalized linear model (~ Treatment) between the expression count. Finally, differential expression analysis was performed

between ConR versus LCR, ConS versus LCS, Con R versus ConS, and LCR versus LCS, and differential expressions were identified by applying multiple testing correction using Benjamin-Hockberg procedure⁸⁶.

Quantitative reverse transcription PCR (qRT-PCR). To validate the RNA-seq data for representative genes, quantitative real-time reverse transcriptase-polymerase chain reaction (qRT-PCR) was performed using a QuantStudio 3 real-time PCR system and the PowerUP™ SYBR Green pre-formulated 2× master mix (Applied Biosystems, Foster City, CA). Total RNA was treated with DNase I (Invitrogen, Carlsbad, CA) to remove contaminating genomic DNA before first-strand cDNA synthesis. First-strand cDNA was synthesized using 5 µg of total RNA and the SuperScript® III First-Strand Synthesis System (Thermo Fisher, Waltham, MA) following the manufacturer's instructions. First-strand cDNA was used in the real-time qRT-PCR reaction containing 2xSYBR Green Master Mix, 500 nM forward, and reverse gene-specific primers in a 20 µL reaction volume. Gene-specific sense and antisense primers 5'-ttggctcctgggactcctaac-3' and 5'-ggccagattgcagtgtagagtttc-3' for *GLR3.1*, 5'-tcattctccatgctcctcaaaaggc-3' and 5'-tctccagttgggccattgtgtc-3' for *CNGC2*, 5'-gcgactcgaggtgtgaatgaagag-3' and 5'-aatggaaccgcccgaacaagac-3' for *CNGC17*, and 5'-tgctgcaattccagaggcttg-3' and 5'-tcacagttgtgcaaccaatgtc-3' were used to amplify *CaE1*. The internal control, eukaryotic elongation factor (*EF1A*) was used as a housekeeping gene and amplified using sense 5'-catcaacatcgtgtcatcg and antisense 5'-gatgcctccaagctttaga-3' primers. Gene expression in the untreated samples were used as a calibrator, and blank (without template) was used as a reference control. The qPCR parameters were as follows: 95°C for 30 s, 40 cycles of 95 °C for 10 s, 60 °C for 30 s, and a final incubation at 72 °C for 5 min followed by melting curve analysis. Relative expression levels based on fold changes were calculated using the $\Delta\Delta CT$ method⁸⁷ available with the QuantStudio3 software (Applied Biosystems, Foster City, CA, USA) and in MS-Excel (Microsoft Corp, Seattle, WA).

Gene annotation. Coding sequences (CDS) of *Eragrostis tef* were annotated by comparing it to the genome sequences of *Setaria italica* (GCF_000263155.2), *Oryza sativa*⁸⁸, and *Sorghum bicolor* (GCF_000003195.3). The CDS of *E. tef* were compared to *S. italica*, *O. sativa*, and *S. bicolor* using Blastx. A CDS was considered significant with *e*-value < 0.00001. Significant hits were first annotated by comparison to *S. italica* (25,876 significant CDS), then to *O. sativa* (873 additional CDS) and *S. bicolor* (483 additional CDS). A total of 94.6% of the CDS of *E. tef* had a significant hit to a CDS of these three genomes, and the corresponding gene annotations were used.

GO analysis. Go analysis was performed using the agriGO⁸⁹. Signature genes from the RNAseq analysis were used as an INPUT, and significantly enriched pathways and/or families were selected based on molecular function, cellular structure, and biological process category.

Data analysis. Treatments were replicated four times, and two independent experiments were conducted. Data were analyzed by the one-way ANOVA using the PROC GLM procedure in SAS⁹⁰. After the significant F-tests, the Tukey's multiple comparisons⁹² were used to separate the means ($P \leq 0.05$). Values represent mean \pm SD of six (Figs. 1B,C) and four (Fig. 2) biological replicates.

Statement on ethics and approvals to use *tef*. *Tef* is primarily cultivated in East Africa and is becoming popular in several countries including South Africa, Australia, and the U.S. The *tef* accessions used in this study was obtained from Dr. John Cushman at the University of Nevada Reno. All methods are performed in accordance with relevant guidelines and regulations.

Data availability

Sequence data files have been stored at <https://www.ncbi.nlm.nih.gov/geo/query/acc.cgi?acc=GSE201043>.

Received: 25 April 2022; Accepted: 7 November 2022

Published online: 15 November 2022

References

- Thor, K. Calcium—Nutrient and messenger. *Front. Plant Sci.* **10**, 440 (2019).
- Lincoln, T., Eduardo, Z., Møller, I. M. & Murphy, A. S. *Fundamentals of Plant Physiology* 450 (Oxford University Press, 2018).
- Ranty, B. *et al.* Calcium sensors as key hubs in plant responses to biotic and abiotic stresses. *Front. Plant Sci.* **7**, 327 (2016).
- White, P. J. & Broadley, M. R. Calcium in plants. *Ann. Bot.* **92**, 487–511 (2003).
- Liu, K.-H. *et al.* Discovery of nitrate–CPK–NLP signalling in central nutrient–growth networks. *Nature* **545**, 311–316 (2017).
- Tang, R.-J., Wang, C., Li, K. & Luan, S. The CBL–CIPK calcium signaling network: Unified paradigm from 20 years of discoveries. *Trends Plant Sci.* **25**, 604–617 (2020).
- Toyota, M. *et al.* Glutamate triggers long-distance, calcium-based plant defense signaling. *Science* **361**, 1112–1115 (2018).
- Weiland, M., Mancuso, S. & Baluska, F. Signalling via glutamate and GLRs in Arabidopsis thaliana. *Funct. Plant Biol.* **43**, 1–25 (2015).
- Ortiz-Ramírez, C. *et al.* GLUTAMATE RECEPTOR-LIKE channels are essential for chemotaxis and reproduction in mosses. *Nature* **549**, 91–95 (2017).
- Salvador-Recatalà, V. New roles for the GLUTAMATE RECEPTOR-LIKE 3.3, 3.5, and 3.6 genes as on/off switches of wound-induced systemic electrical signals. *Plant Signal. Behav.* **11**, e1161879 (2016).
- Nguyen, C. T., Kurenda, A., Stolz, S., Chételat, A. & Farmer, E. E. Identification of cell populations necessary for leaf-to-leaf electrical signaling in a wounded plant. *Proc. Natl. Acad. Sci.* **115**, 10178–10183 (2018).
- Wang, Y. *et al.* CNGC2 is a Ca²⁺ influx channel that prevents accumulation of apoplastic Ca²⁺ in the leaf. *Plant Physiol.* **173**, 1342–1354 (2017).
- Lu, M. *et al.* AtCNGC2 is involved in jasmonic acid-induced calcium mobilization. *J. Exp. Bot.* **67**, 809–819 (2016).
- Kong, X., Xu, L. & Jamieson, P. Plant sense: The rise of calcium channels. *Trends Plant Sci.* **25**, 838–841 (2020).

15. Ma, Y. & Berkowitz, G. A. Multimeric CAX complexes and Ca²⁺ signaling—beyond humdrum housekeeping. *J. Exp. Bot.* **68**, 3997–3999 (2017).
16. Jammes, F., Hu, H. C., Villiers, F., Bouten, R. & Kwak, J. M. Calcium-permeable channels in plant cells. *FEBS J.* **278**, 4262–4276 (2011).
17. Yadav, A. K. *et al.* A rice tonoplast calcium exchanger, OsCCX2 mediates Ca²⁺/cation transport in yeast. *Sci. Rep.* **5**, 1–15 (2015).
18. Wang, Y., Martins, L. B., Sermons, S. & Balint-Kurti, P. Genetic and physiological characterization of a calcium deficiency phenotype in maize. *G3 Genes Genomes Genet.* **10**, 1963–1970 (2020).
19. da Silva, D. L., de Mello Prado, R., Tenesaca, L. F. L., da Silva, J. L. F. & Mattiuz, B.-H. Silicon attenuates calcium deficiency by increasing ascorbic acid content, growth and quality of cabbage leaves. *Sci. Rep.* **11**, 1–9 (2021).
20. Ranjitha, K. *et al.* Integrating calcium chloride treatment with polypropylene packaging improved the shelf life and retained the quality profile of minimally processed cabbage. *Food Chem.* **256**, 1–10 (2018).
21. Almeida, H. J. D. *et al.* Nutritional and visual diagnosis in broccoli (*Brassica oleracea* var *italica* L.). Plants: Disorders in physiological activity, nutritional efficiency and metabolism of carbohydrates. *Agronomy* **10**, 1572 (2020).
22. Tan, W., WeiMeng, Q., Brestic, M., Olsovska, K. & Yang, X. Photosynthesis is improved by exogenous calcium in heat-stressed tobacco plants. *J. Plant Physiol.* **168**, 2063–2071 (2011).
23. Xu, C., Li, X. & Zhang, L. The effect of calcium chloride on growth, photosynthesis, and antioxidant responses of *Zoysia japonica* under drought conditions. *PLoS ONE* **8**, e68214 (2013).
24. Cheng, T.-S., Hung, M.-J., Cheng, Y.-I. & Cheng, L.-J. Calcium-induced proline accumulation contributes to amelioration of NaCl injury and expression of glutamine synthetase in greater duckweed (*Spirodela polyrhiza* L.). *Aquat. Toxicol.* **144**, 265–274 (2013).
25. Ahmad, P. *et al.* Alleviation of cadmium toxicity in *Brassica juncea* L. (Czern. & Coss) by calcium application involves various physiological and biochemical strategies. *PLoS ONE* **10**, e0114571 (2015).
26. Ligaba-Osena, A. *et al.* Loss-of-function mutation of the calcium sensor CBL 1 increases aluminum sensitivity in Arabidopsis. *New Phytol.* **214**, 830–841 (2017).
27. Li, L., Kim, B.-G., Cheong, Y. H., Pandey, G. K. & Luan, S. A Ca²⁺ signaling pathway regulates a K⁺ channel for low-K response in Arabidopsis. *Proc. Natl. Acad. Sci.* **103**, 12625–12630 (2006).
28. Gratz, R., von der Mark, C., Ivanov, R. & Brumbarova, T. Fe acquisition at the crossroad of calcium and reactive oxygen species signaling. *Curr. Opin. Plant Biol.* **63**, 102048 (2021).
29. Matthus, E. *et al.* DORN1/P2K1 and purino-calcium signalling in plants: making waves with extracellular ATP. *Ann. Bot.* **124**, 1227–1242 (2019).
30. Martín-Barranco, A., Spielmann, J., Dubeaux, G., Vert, G. & Zelazny, E. Dynamic control of the high-affinity iron uptake complex in root epidermal cells. *Plant Physiol.* **184**, 1236–1250 (2020).
31. Assefa, K., Chanyalew, S., Tadele, Z. Tef, *eragrostis tef* (Zucc.) trotter. *Millet Sorghum Biol. Genet. Improv.* 226–266 (2017).
32. Numan, M. *et al.* From traditional breeding to genome editing for boosting productivity of the ancient grain tef [*Eragrostis tef* (Zucc.) Trotter]. *Plants* **10**, 628 (2021).
33. Barretto, R. *et al.* Tef (*Eragrostis tef*) processing, utilization and future opportunities: a review. *Int. J. Food Sci. Technol.* **56**, 3125–3137 (2021).
34. Chanyalew, S. *et al.* Significance and prospects of an orphan crop tef. *Planta* **250**, 753–767 (2019).
35. Ligaba-Osena, A. *et al.* Grain mineral nutrient profiling and iron bioavailability of an ancient crop tef (*Eragrostis tef*). *Aust. J. Crop Sci.* **15**(10), 1314–1324 (2021).
36. Mohammed, M. I., Mustafa, A. I. & Osman, G. A. Evaluation of wheat breads supplemented with Tef (*Eragrostis tef* (ZUCC.) Trotter) grain flour. *Aust. J. Crop Sci.* **3**, 207–212 (2009).
37. Puranik, S. *et al.* Harnessing finger millet to combat calcium deficiency in humans: Challenges and prospects. *Front. Plant Sci.* **8**, 1311 (2017).
38. VanBuren, R. *et al.* Exceptional subgenome stability and functional divergence in the allotetraploid Ethiopian cereal tef. *Nat. Commun.* **11**, 1–11 (2020).
39. Kim, D., Paggi, J. M., Park, C., Bennett, C. & Salzberg, S. L. Graph-based genome alignment and genotyping with HISAT2 and HISAT-genotype. *Nat. Biotechnol.* **37**, 907–915 (2019).
40. Anders, S., Pyl, P. & Huber, W. HTSeq—a Python framework to work with high-throughput sequencing data. *Bioinformatics* <https://doi.org/10.1093/bioinformatics/btu638> (2014).
41. Love, M. I., Huber, W. & Anders, S. Moderated estimation of fold change and dispersion for RNA-seq data with DESeq2. *Genome Biol.* **15**, 1–21 (2014).
42. Team, R. C. R. *A Language and Environment for Statistical Computing*. R Foundation for Statistical Computing, Vienna, Austria. <http://www.R-project.org/> (2013).
43. Ligaba-Osena, A. *et al.* Grain mineral nutrient profiling and iron bioavailability of an ancient crop tef (*Eragrostis tef*). *Aust. J. Crop Sci.* **15**, 1314–1324 (2021).
44. Sun, H.-Y. *et al.* Transcriptomics reveals the ERF2-bHLH2-CML5 module responses to H₂S and ROS in postharvest calcium deficiency apples. *Int. J. Mol. Sci.* **22**, 13013 (2021).
45. Bindra, A. *Iron Chlorosis in Horticultural and Field Crops* (Kalyani Publishers, 1983).
46. Fageria, N. & Baligar, V. Growth and nutrient concentrations of common bean, lowland rice, corn, soybean, and wheat at different soil pH on an Inceptisol. *J. Plant Nutr.* **22**, 1495–1507 (1999).
47. Knight, H. *International Review of Cytology* Vol. 195, 269–324 (Elsevier, 1999).
48. Dodd, A. N., Kudla, J. & Sanders, D. The language of calcium signaling. *Annu. Rev. Plant Biol.* **61**, 593–620 (2010).
49. Demidchik, V., Shabala, S., Isayenkov, S., Cuin, T. A. & Pottosin, I. Calcium transport across plant membranes: Mechanisms and functions. *New Phytol.* **220**, 49–69. <https://doi.org/10.1111/nph.15266> (2018).
50. Yadav, A. K. *Calcium Transport Elements in Plants* 103–128 (Elsevier, 2021).
51. Teardo, E. *et al.* A chloroplast-localized mitochondrial calcium uniporter transduces osmotic stress in Arabidopsis. *Nat. Plants* **5**, 581–588 (2019).
52. Selles, B., Michaud, C., Xiong, T. C., Leblanc, O. & Ingouff, M. Arabidopsis pollen tube germination and growth depend on the mitochondrial calcium uniporter complex. *New Phytol.* **219**, 58–65 (2018).
53. De Stefani, D., Patron, M. & Rizzuto, R. Structure and function of the mitochondrial calcium uniporter complex. *Biochim. Biophys. Acta BBA-Mol. Cell Res.* **1853**, 2006–2011 (2015).
54. Li, Z. *et al.* CCX1, a putative cation/Ca²⁺ exchanger, participates in regulation of reactive oxygen species homeostasis and leaf senescence. *Plant Cell Physiol.* **57**, 2611–2619. <https://doi.org/10.1093/pcp/pcw175> (2016).
55. Singh, A. *et al.* Genome-wide expressional and functional analysis of calcium transport elements during abiotic stress and development in rice. *FEBS J.* **281**, 894–915 (2014).
56. Yang, J. *et al.* Cation/Ca²⁺ exchanger 1 (MdCCX1), a plasma membrane-localized Na⁺ transporter, enhances plant salt tolerance by inhibiting excessive accumulation of Na⁺ and reactive oxygen species. *Front. Plant Sci.* <https://doi.org/10.3389/fpls.2021.746189> (2021).
57. Amagaya, K., Shibuya, T., Nishiyama, M., Kato, K. & Kanayama, Y. Characterization and expression analysis of the Ca²⁺/cation antiporter gene family in tomatoes. *Plants* **9**, 25 (2020).
58. Nitsche, J. *et al.* Structural basis for activation of plasma-membrane Ca²⁺-ATPase by calmodulin. *Commun. Biol.* **1**, 1–10 (2018).

59. Iwano, M. *et al.* A pollen coat–inducible autoinhibited Ca²⁺-ATPase expressed in stigmatic papilla cells is required for compatible pollination in the Brassicaceae. *Plant Cell* **26**, 636–649 (2014).
60. Koh, S. *et al.* An oligopeptide transporter gene family in Arabidopsis. *Plant Physiol.* **128**, 21–29 (2002).
61. Mendoza-Cózatl, D. G. *et al.* OPT3 is a component of the iron–signaling network between leaves and roots and misregulation of OPT3 leads to an over-accumulation of cadmium in seeds. *Mol. Plant* **7**, 1455–1469 (2014).
62. Zhai, Z. *et al.* OPT3 is a phloem–specific iron transporter that is essential for systemic iron signaling and redistribution of iron and cadmium in Arabidopsis. *Plant Cell* **26**, 2249–2264 (2014).
63. Bashir, K. *et al.* Iron deficiency regulated OsOPT7 is essential for iron homeostasis in rice. *Plant Mol. Biol.* **88**, 165–176 (2015).
64. Osawa, H., Stacey, G. & Gassmann, W. ScOPT1 and AtOPT4 function as proton-coupled oligopeptide transporters with broad but distinct substrate specificities. *Biochem. J.* **393**, 267–275 (2006).
65. Cagnac, O., Bourbonloux, A., Chakrabarty, D., Zhang, M.-Y. & Delrot, S. AtOPT6 transports glutathione derivatives and is induced by primisulfuron. *Plant Physiol.* **135**, 1378–1387 (2004).
66. Roberts, L. A., Pierson, A. J., Panaviene, Z. & Walker, E. L. Yellow stripe1. Expanded roles for the maize iron-phytosiderophore transporter. *Plant Physiol.* **135**, 112–120 (2004).
67. Inoue, H. *et al.* Rice OsYSL15 is an iron-regulated iron (III)-deoxymugineic acid transporter expressed in the roots and is essential for iron uptake in early growth of the seedlings. *J. Biol. Chem.* **284**, 3470–3479 (2009).
68. Ishimaru, Y. *et al.* Rice metal-nicotianamine transporter, OsYSL2, is required for the long-distance transport of iron and manganese. *Plant J.* **62**, 379–390 (2010).
69. Zang, J. *et al.* Maize YSL2 is required for iron distribution and development in kernels. *J. Exp. Bot.* **71**, 5896–5910 (2020).
70. Waters, B. M. *et al.* Mutations in Arabidopsis yellow stripe-like1 and yellow stripe-like3 reveal their roles in metal ion homeostasis and loading of metal ions in seeds. *Plant Physiol.* **141**, 1446–1458 (2006).
71. DiDonato, R. J. Jr., Roberts, L. A., Sanderson, T., Eisle, R. B. & Walker, E. L. Arabidopsis Yellow Stripe-Like2 (YSL2): A metal-regulated gene encoding a plasma membrane transporter of nicotianamine–metal complexes. *Plant J.* **39**, 403–414 (2004).
72. Zhang, Y., Xu, Y. H., Yi, H. Y. & Gong, J. M. Vacuolar membrane transporters OsVIT1 and OsVIT2 modulate iron translocation between flag leaves and seeds in rice. *Plant J.* **72**, 400–410 (2012).
73. Connorton, J. M. *et al.* Altering expression of a vacuolar iron transporter doubles iron content in white wheat flour. *bioRxiv*, 131888 (2017).
74. Barberon, M. *et al.* Polarization of IRON-REGULATED TRANSPORTER 1 (IRT1) to the plant–soil interface plays crucial role in metal homeostasis. *Proc. Natl. Acad. Sci.* **111**, 8293–8298 (2014).
75. Gratz, R. *et al.* CIPK11-dependent phosphorylation modulates FIT activity to promote Arabidopsis iron acquisition in response to calcium signaling. *Develop. Cell* **48**, 726–740 (2019).
76. Khan, I. *et al.* Calcium-promoted interaction between the C2-domain protein EHB1 and metal transporter IRT1 inhibits Arabidopsis iron acquisition. *Plant Physiol.* **180**, 1564–1581 (2019).
77. Urquhart, W., Chin, K., Ung, H., Moeder, W. & Yoshioka, K. The cyclic nucleotide-gated channels AtCNGC11 and 12 are involved in multiple Ca²⁺-dependent physiological responses and act in a synergistic manner. *J. Exp. Bot.* **62**, 3671–3682 (2011).
78. Tian, W. *et al.* A calmodulin-gated calcium channel links pathogen patterns to plant immunity. *Nature* **572**, 131–135 (2019).
79. Wu, Y. *et al.* P2K1 receptor, heterotrimeric Gα protein and CNGC2/4 are involved in extracellular ATP-promoted ion influx in the pollen of Arabidopsis thaliana. *Plants* **10**, 1743 (2021).
80. Lindsey III, B. E., Rivero, L., Calhoun, C. S., Grotewold, E., Brkljacic, J. Standardized method for high-throughput sterilization of Arabidopsis seeds. *JoVE J. Vis. Exp.* e56587 (2017).
81. Hoagland, D. R., Arnon, D. I. The water-culture method for growing plants without soil. *Circular. California agricultural experiment station* **347** (1950).
82. Joshi, N. A. & Fass, J. N. Sickle: A sliding-window, adaptive, quality-based trimming tool for FastQ files (Version 1.33) [Software]. Available at <https://github.com/najoshi/sickle> (2011).
83. Sirén, J., Välimäki, N. & Mäkinen, V. HISAT2-fast and sensitive alignment against general human population. *IEEE/ACM Trans. Comput. Biol. Bioinf.* **11**, 375–388 (2014).
84. Putri, G. H., Anders, S., Pyl, P. T., Pimanda, J. E. & Zanini, F. Analysing high-throughput sequencing data in Python with HTSeq 2.0. *Bioinformatics* **38**, 2943–2945 (2022).
85. Love, M., Anders, S. & Huber, W. Differential analysis of count data—the DESeq2 package. *Genome Biol.* **15**, 10.1186 (2014).
86. Benjamini, Y. & Hochberg, Y. Controlling the false discovery rate: a practical and powerful approach to multiple testing. *J. R. Stat. Soc. Ser. B (Methodol.)* **57**, 289–300 (1995).
87. Livak, K. J. & Schmittgen, T. D. Analysis of relative gene expression data using real-time quantitative PCR and the 2[−]ΔΔCT method. *Methods* **25**, 402–408 (2001).
88. Kawahara, Y. *et al.* Improvement of the *Oryza sativa* Nipponbare reference genome using next generation sequence and optical map data. *Rice* **6**, 1–10 (2013).
89. Tian, T. *et al.* agriGO v2 0: A GO analysis toolkit for the agricultural community, 2017 update. *Nucl. Acids Res.* **45**, W122–W129 (2017).
90. Lee, J. Analysis of covariance by the SAS GLM procedure. *Comput. Biol. Med.* **17**, 221–225 (1987).
91. Wilkinson, L. *Systat. Wiley Interdiscip. Rev. Comput. Stat.* **2**, 256–257 (2010).
92. Keselman, H. & Rogan, J. C. The Tukey multiple comparison test: 1953–1976. *Psychol. Bull.* **84**, 1050 (1977).

Acknowledgements

This study was supported by The University of North Carolina at Greensboro (Grant # 133504 to A.L.-O.). Authors thank Dr. Ramji Bhandari for helpful discussions, Dr. Patricia Baldrich (Donald Danforth Plant Science Center) for help with data analysis, and Dr. John Cushman (university of Nevada Reno) for providing seeds of tef accessions.

Author contributions

A.L.-O. conceived the project. S.C.C., M.S., W.G. and A.L.-O. designed the experiments. M.S., W.G., X.W., and S.C.-C. collected and analyzed the data. D.J. and L.M.B. performed the bioinformatic analysis. M.S., M.N. and A.L.-O. wrote the manuscript. All authors have reviewed the manuscript before submission.

Competing interests

The authors declare no competing interests.

Additional information

Supplementary Information The online version contains supplementary material available at <https://doi.org/10.1038/s41598-022-23844-z>.

Correspondence and requests for materials should be addressed to A.L.-O.

Reprints and permissions information is available at www.nature.com/reprints.

Publisher's note Springer Nature remains neutral with regard to jurisdictional claims in published maps and institutional affiliations.



Open Access This article is licensed under a Creative Commons Attribution 4.0 International License, which permits use, sharing, adaptation, distribution and reproduction in any medium or format, as long as you give appropriate credit to the original author(s) and the source, provide a link to the Creative Commons licence, and indicate if changes were made. The images or other third party material in this article are included in the article's Creative Commons licence, unless indicated otherwise in a credit line to the material. If material is not included in the article's Creative Commons licence and your intended use is not permitted by statutory regulation or exceeds the permitted use, you will need to obtain permission directly from the copyright holder. To view a copy of this licence, visit <http://creativecommons.org/licenses/by/4.0/>.

© The Author(s) 2022